Electronic Supplementary Material (ESI) for ChemComm.
This journal is © The Royal Society of Chemistry 2015

*Supporting Information for*

# Uniaxial Magnetic Anisotropy of Square-Planar Chromium(II) Complexes Revealed by Magnetic and HF-EPR Studies

Yi-Fei Deng,‡[a] Tian Han,‡[a] Zhenxing Wang,[b] Zhongwen Ouyang,[b] Bing Yin,*[c] Zhiping Zheng,[d] J. Krzystek,[e] Yan-Zhen Zheng*[a]

[a] Centre for Applied Chemical Research, Frontier Institute of Science and Technology, and MOE Key Laboratory for Nonequilibrium Synthesis, College of Science, Xi'an Jiaotong University, Xi'an 710054, China.

[b] National High Magnetic Field Centre, Huazhong University of Science and Technology, Wuhan 430074, China.

[c] MOE Key Laboratory of Synthetic and Natural Functional Molecule Chemistry, College of Chemistry and Materials Science, Northwest University, Xi'an 710069, China

[d] Department of Biochemistry, The University of Arizona, Tucson Arizona 85721, USA

[e] National High Magnetic Field Laboratory, Florida State University, Tallahassee, Florida 32310, USA.

‡ These authors contributed equally to this work.

Email: zheng.yanzhen@mail.xjtu.edu.cn (Y.Z.Z.) rayinyin@nwu.edu.cn (B.Y.)

## Table of contents

1. General Experimental Section .....2

2. X-Ray Crystallography Data.....2

3. Powder X-ray Diffraction .....5

4. Magnetic Data .....6

5. HF-EPR Measurements .....11

6. Theoretical Calculations .....12

## 1. General Experimental Section

All chemicals were commercially available and were used as received. All the solvents were dehydrated and deoxygenated by Solvent Purification Systems prior to use. All manipulations were performed under a dry and oxygen-free argon atmosphere by using Schlenk techniques or in a glovebox.

**Preparation of $Cr^{II}(N(TMS)_2)_2(py)_2$ (1)**:

A mixture of $LiN(SiMe_3)_2)_2$ (67 mg, 0.4 mmol), anhydrous chromium(II) chloride ($CrCl_2$) (24 mg, 0.2 mmol) and pyridine (32 μL, 0.4 mmol) were dissolved in THF (4 mL) and then stirred at room temperature for 12 h. After removal of solvent at pump vacuum, 6 mL pentane was added and all insoluble solids were removed by filtration. Light yellow crystalline **1** was obtained (40 mg, 38%) by allowing the resulting solution to stand at −35 °C within 2 days.

**Preparation of $Cr^{II}(N(TMS)_2)_2(THF)_2$ (2)**:

$LiN(SiMe_3)_2)_2$ (100.4 mg, 0.6 mmol) and anhydrous chromium(III) chloride ($CrCl_3$) (31.7 mg, 0.2 mmol) were added into a Schlenk tube, followed by injection of THF (5 ml), and the mixture was stirred overnight. The resulting solution was distillated to dryness in vacuo. The residue was taken up in pentane and filtered through the Celite. The filtrate was cooled to −35 °C, which gave purple crystals (ca. 30 % yield, based on Cr). The product can be also obtained from $CrCl_2$ by a similar procedure described in the literature.[1]

## 2. X-Ray Crystallography Data

Crystal data of **1** and **2** were collected on a Bruker Apex CCD area-detector diffractometer using MoK$\alpha$ ($\lambda$ = 0.71073 Å) radiation. Absorption corrections were applied using the multi-scan program SADABS.[2] The structures were solved using direct methods and refined with a full-matrix least-squares technique using SHELXTL programpackage.[3] Anisotropic thermal parameters were assigned to all non-hydrogen atoms. The hydrogen atoms were generated geometrically. Data collection and structural refinement parameters are given in Table S1 and selected bond distances and angles are given in Table S2. CCDC-1057925 (**1**) contains the crystallographic data that can be obtained via www.ccdc.cam.ac.uk/conts/retrieving.html (or from the Cambridge Crystallographic Data Centre, 12, Union Road, Cambridge CB21EZ, UK; fax: (+44) 1223-336-033; or deposit@ccdc.cam.ac.uk).

**Table S1**. Crystal data and structure refinement for **1** and **2**.

| | **1** | **2** |
|---|---|---|
| formula | $C_{22}H_{46}CrN_4Si_4$ | $C_{20}H_{52}CrN_2O_2Si_4$ |
| $M$/g mol$^{-1}$ | 531 | 517 |
| crystal system | Triclinic | Triclinic |
| space group | $P$-1 | $P$-1 |
| $a$, Å | 10.972(16) | 10.920(4) |
| $b$, Å | 11.699(16) | 11.513(4) |
| $c$, Å | 13.519(19) | 13.403(4) |
| $\alpha$, deg | 99.28(2) | 70.212(4) |
| $\beta$, deg | 95.81(2) | 78.069(4) |
| $\gamma$, deg | 115.672(18) | 84.626(5) |
| $V$, Å$^3$ | 1515(4) | 1550.7(9) |
| Z | 2 | 2 |
| $d_{cal}$/g cm$^{-3}$ | 1.164 | 1.107 |
| temperature, K | 296(2) | 296(2) |
| $\theta$ range | 1.56 – 25.00° | 1.64 – 25.00° |
| completeness | 99.3% | 98.0% |
| residual map, e Å$^{-3}$ | 0.220 and –0.233 | 1.021 and –0.292 |
| Goodness-of-fit on $F^2$ | 1.014 | 1.079 |
| final indices [$I>2\sigma(I)$] | $R_1$ = 0.0342, $wR_2$ = 0.0841 | $R_1$ = 0.0596, $wR_2$ = 0.1623 |
| $R$ indices (all data) | $R_1$ = 0.0538, $wR_2$ = 0.0922 | $R_1$ = 0.0827, $wR_2$ = 0.1755 |

**Table S2.** Selected bond lengths (Å) and angles (°) for complexes **1** and **2**.

| **1** | | | | **2** | | | |
|---|---|---|---|---|---|---|---|
| Bonds | Å | Angles | ° | Bonds | Å | Angles | ° |
| Cr(1)-N(1) | 2.044(3) | N(3)-Cr(1)-N(1) | 178.85(8) | Cr(1)-N(1) | 2.070(3) | N(1)-Cr(1)-N(2) | 178.89(12) |
| Cr(1)-N(2) | 2.099(3) | N(3)-Cr(1)-N (4) | 90.33(14) | Cr(1)-N(2) | 2.078(3) | N(1)-Cr(1)-O(2) | 89.54(12) |
| Cr(1)-N(3) | 2.040(3) | N(1)-Cr(1)-N(4) | 89.40(14) | Cr(1)-O(1) | 2.089(3) | N(2)-Cr(1)-O(2) | 90.42(12) |
| Cr(1)-N(4) | 2.099(3) | N(3)-Cr(1)-N(2) | 90.90(14) | Cr(1)-O(2) | 2.087(3) | N(1)-Cr(1)-O(1) | 90.21(12) |
| | | N(1)-Cr(1)-N(2) | 89.37(14) | | | N(2)-Cr(1)-O(1) | 89.86(12) |
| | | N(4)-Cr(1)-N(2) | 178.76(8) | | | O(2)-Cr(1)-O(1) | 178.31(12) |
| | | N(1)-N(2)-N(3) | 88.28(9) | | | O(1)-N(1)-O(2) | 90.64(12) |
| | | N(2)-N(3)-N(4) | 91.01(9) | | | N(1)-O(2)-N(2) | 89.66(12) |
| | | N(3)-N(4)-N(1) | 88.54(9) | | | O(2)-N(2)-O(1) | 90.11(12) |
| | | N(4)-N(1)-N(2) | 92.16(9) | | | N(2)-O(1)-N(1) | 89.53(13) |

**Table S3**. The best results fitted for **1** under 1500 Oe dc field and **2** under 2500 Oe dc field by a generalized Debye model.

| **1** | | | **2** | | |
|---|---|---|---|---|---|
| $T$ / K | $\tau$ / s | $\alpha$ | $T$ / K | $\tau$ / s | $\alpha$ |
| 2.0 | $1.23 \times 10^{-3}$ | $8.24 \times 10^{-2}$ | 2.0 | $1.14 \times 10^{-3}$ | 0.17 |
| 2.2 | $8.85 \times 10^{-4}$ | $7.68 \times 10^{-2}$ | 2.2 | $7.10 \times 10^{-4}$ | 0.15 |
| 2.4 | $6.19 \times 10^{-4}$ | $6.95 \times 10^{-2}$ | 2.4 | $4.30 \times 10^{-4}$ | 0.12 |
| 2.6 | $4.61 \times 10^{-4}$ | $6.14 \times 10^{-2}$ | 2.6 | $2.90 \times 10^{-4}$ | 0.10 |
| 2.8 | $3.57 \times 10^{-4}$ | $5.64 \times 10^{-2}$ | 2.8 | $2.10 \times 10^{-4}$ | 0.08 |
| 3.0 | $2.85 \times 10^{-4}$ | $4.96 \times 10^{-2}$ | 3.0 | $1.50 \times 10^{-4}$ | 0.08 |
| 3.2 | $2.33 \times 10^{-4}$ | $4.52 \times 10^{-2}$ | | | |
| 3.4 | $1.91 \times 10^{-4}$ | $4.46 \times 10^{-2}$ | | | |
| 3.6 | $1.61 \times 10^{-4}$ | $3.86 \times 10^{-2}$ | | | |
| 3.8 | $1.39 \times 10^{-4}$ | $3.58 \times 10^{-2}$ | | | |

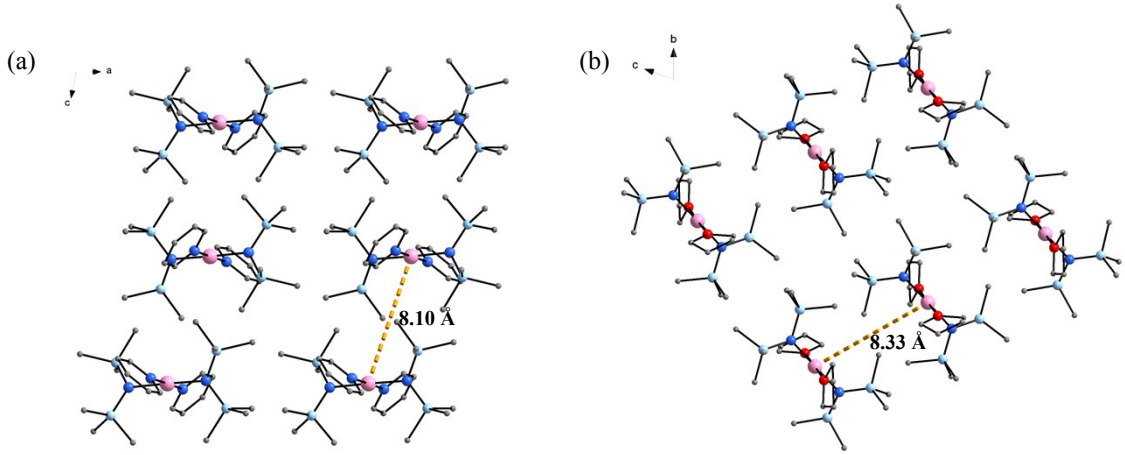


**Figure S1**. (a) Packing arrangement of **1** along the crystallographic b axis; (b) Packing arrangement of **2** along the crystallographic a axis. The dashed lines show the nearest intermolecular Cr···Cr separation. Hydrogen atoms are omitted for clarity.

## 3. Powder X-ray Diffraction

The Powder X-ray diffraction (PXRD) measurements were recorded on a Rigaku Smartlab X-ray diffractometer.

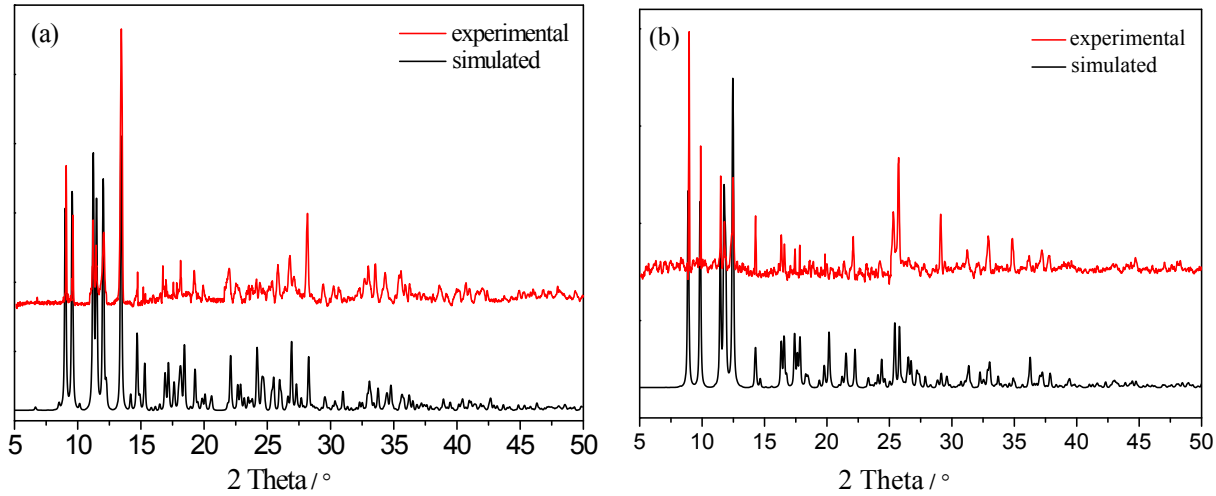


**Figure S2**. The powder X-ray diffractions for **1** (a) and **2** (b). The black curves are calculated from the single crystal data

## 4. Magnetic Data

Magnetic susceptibility measurements on polycrystalline samples of **1** and **2** were carried out on a Quantum Design MPMS-XL7 SQUID magnetometer between 2 to 300 K and ±7 T. Dc susceptibility measurements were collected in the temperature range 2−300 K under a dc field of 1000 Oe. Dc magnetization measurements were obtained in the temperature range 2−5 K under dc fields up to 7 T. Ac susceptibility measurements were performed at frequencies between 1 and 1500 Hz with an ac field of 3.5 Oe. Diamagnetic corrections were calculated from Pascal constants and applied to all the constituent atoms and sample holder.

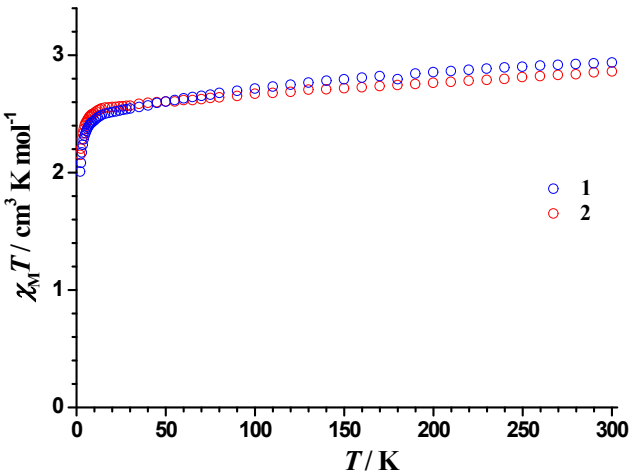


**Figure S3**. $\chi_M T$ versus $T$ plots for **1** and **2** under 1000 Oe dc field.

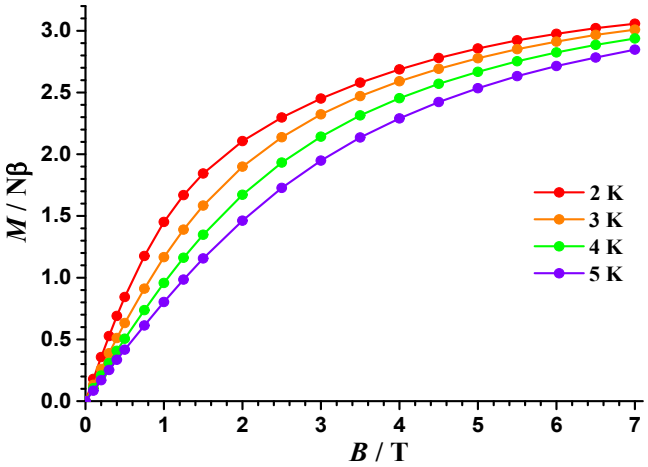


**Figure S4.** Field dependence of the magnetization $M$ at 2, 3, 4 and 5 K for **1**. The lines are guides to the eyes.

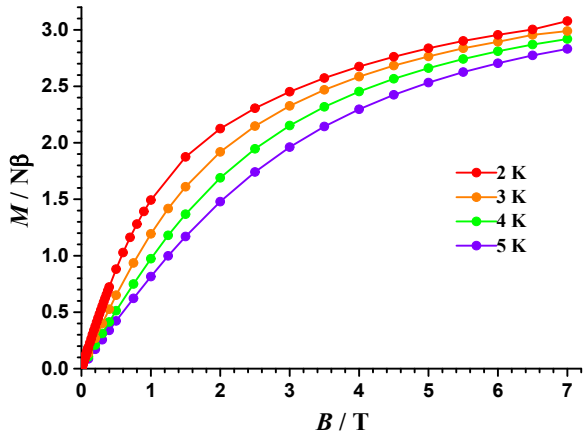


**Figure S5**. Field dependence of the magnetization *M* at 2, 3, 4 and 5 K for **2**. The lines are guides to the eyes.

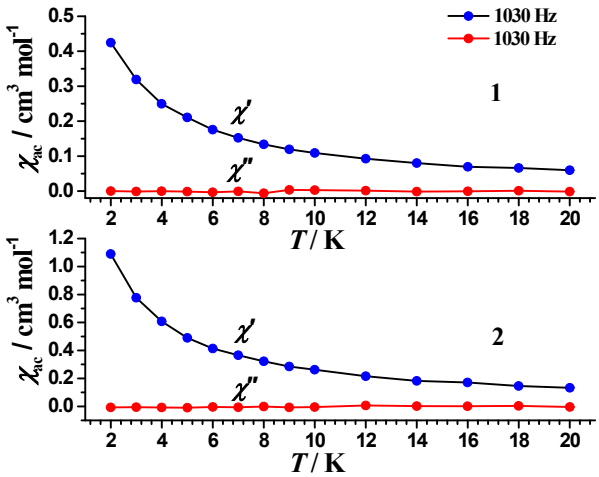


**Figure S6**. Temperature dependence of the in-phase ($\chi'$) and out-of-phase ($\chi''$) ac susceptibility for **1** and **2** under 0 Oe dc field. The lines are guides to the eyes.

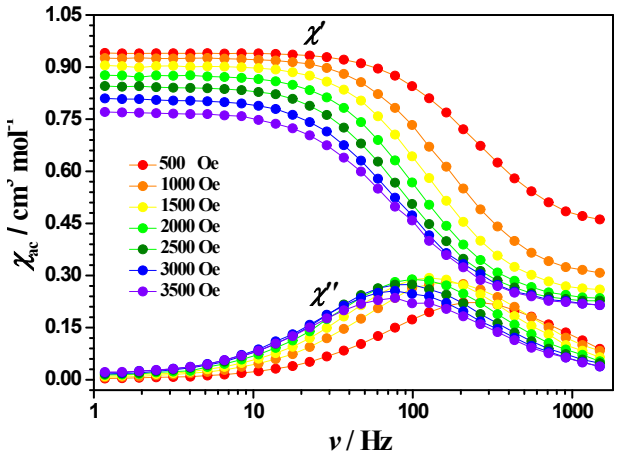


**Figure S7**. Frequency dependence of the in-phase ($\chi'$) and out-of-phase ($\chi''$) ac susceptibility for **1** at 2 K under various dc fields. The lines are guides to the eyes.

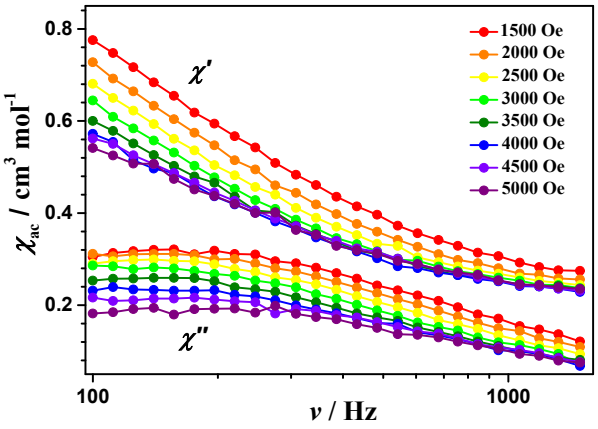


**Figure S8**. Frequency dependence of the in-phase ($\chi'$) and out-of-phase ($\chi''$) ac susceptibility for **2** at 2 K under various dc fields. The lines are guides to the eyes.

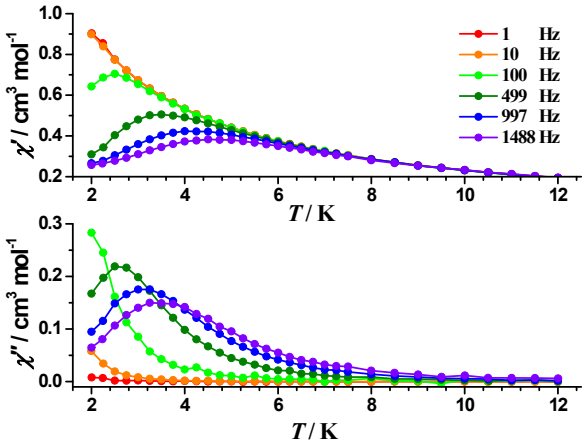


**Figure S9**. Temperature dependence of the in-phase ($\chi'$) and out-of-phase ($\chi''$) ac susceptibility for **1** under 1500 Oe dc field. The lines are guides to the eyes.

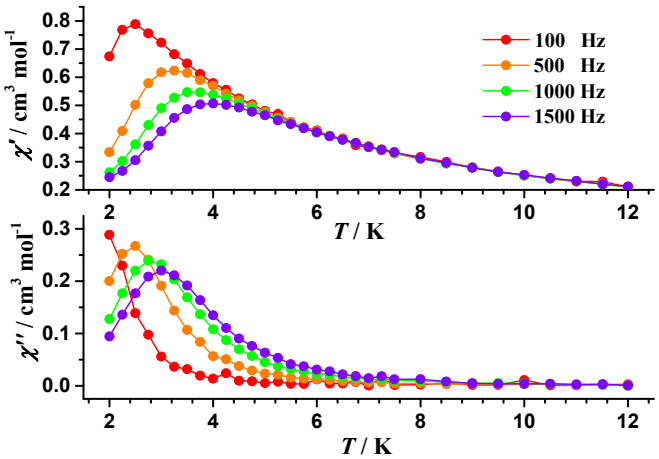


**Figure S10**. Temperature dependence of the in-phase ($\chi'$) and out-of-phase ($\chi''$) ac susceptibility for **2** under 2500 Oe dc field. The lines are guides to the eyes.

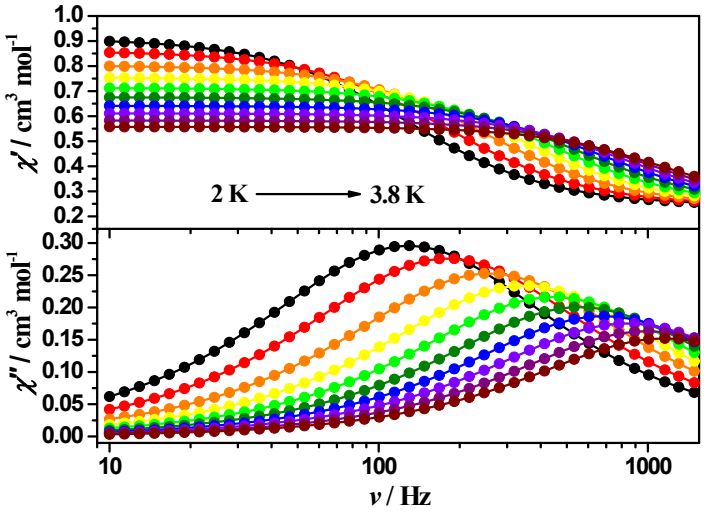


**Figure S11**. Frequency dependence of the in-phase $\chi'$ (top) and out-of-phase $\chi''$ (bottom) components of the alternating-current (ac) susceptibility for the complex **1** measured under 1500 Oe dc field in the temperature range of 2–3.8 K. The lines are guides to the eyes.

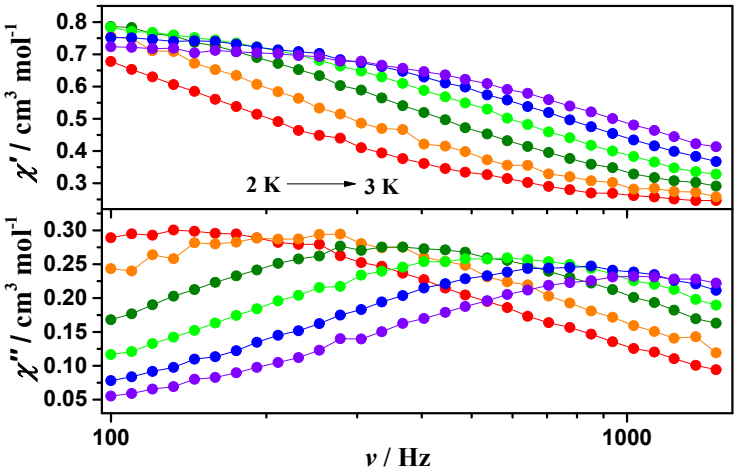


**Figure S12**. Frequency dependence of the in-phase $\chi'$ (top) and out-of-phase $\chi''$ (bottom) components of the alternating-current (ac) susceptibility for the complex **2** measured under 2500 Oe dc field in the temperature range of 2–3 K. The lines are guides to the eyes.

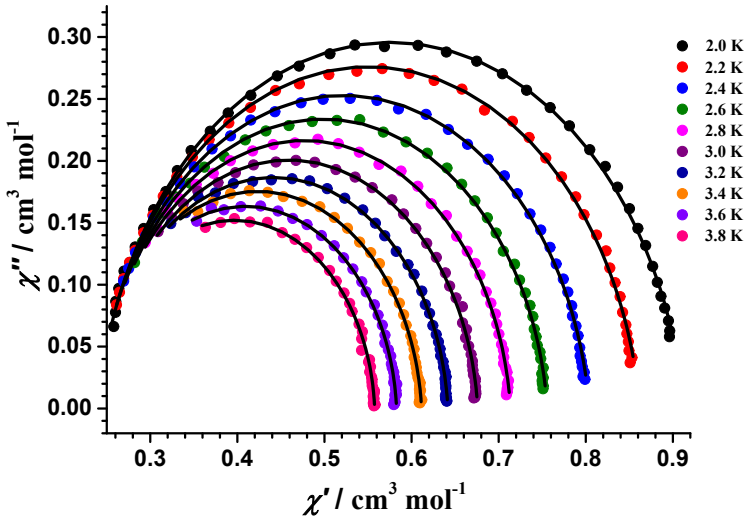


**Figure S13**. Cole-Cole plots for **1** at 1500 Oe dc field. The solid lines represent a fit to the data.

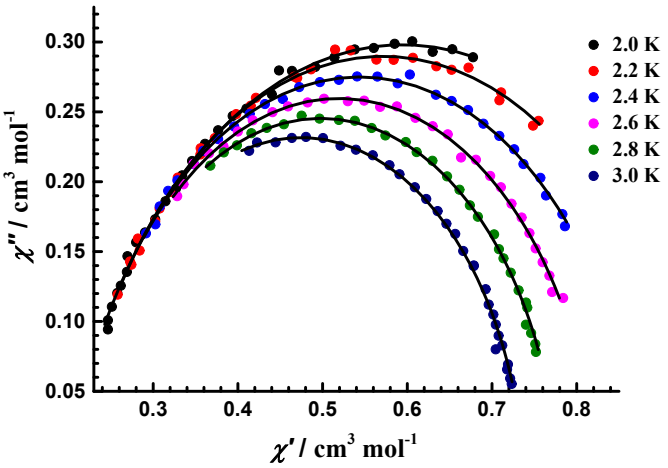


**Figure S14**. Cole-Cole plots for **2** at 2500 Oe dc field. The solid lines represent a fit to the data.

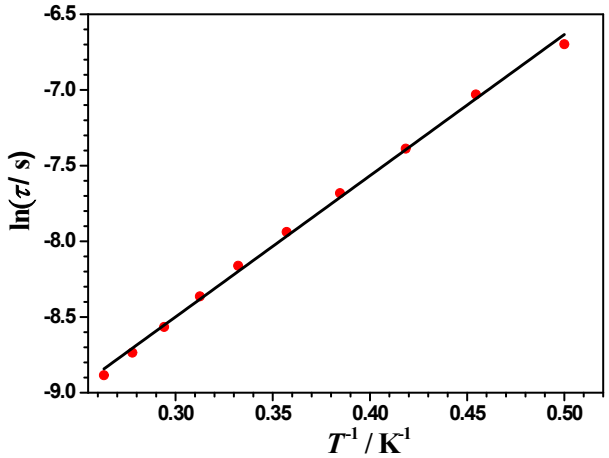


**Figure S15**. Arrhenius plot of $\tau$ data for **1**. The solid line represents the best fit to Arrhenius Law.

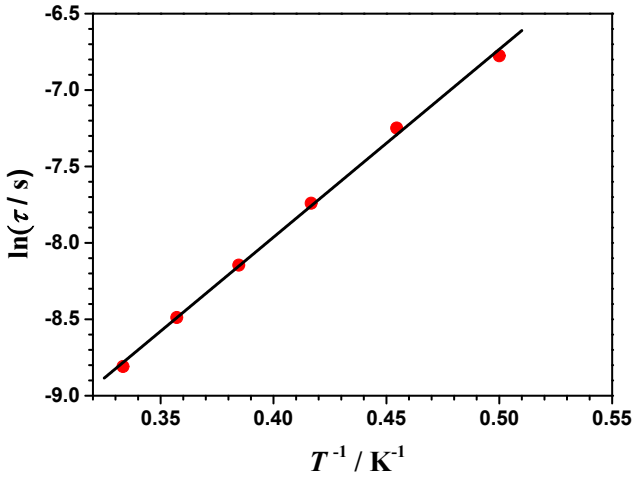


**Figure S16**. Arrhenius plot of $\tau$ data for **2**. The solid line represents the best fit to Arrhenius Law.

## 5. HF-EPR Measurements

HF-EPR measurements were performed on a locally developed spectrometer at Wuhan National High Magnetic Field Centre, using a pulsed magnetic field of up to 30 T.[4] The raw spectra obtained in an absorptive mode were subsequently digitally transformed into a derivative presentation. Simulations and fitting were performed using SPIN developed by Andrew Ozarowski in the National High Magnetic Field Laboratory, USA.

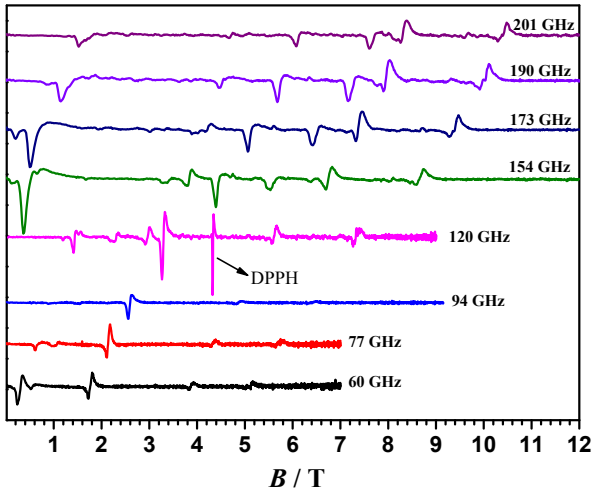


**Figure S17**. Variable-frequency EPR spectra collected on a powder sample of **1** at 4.2 K.

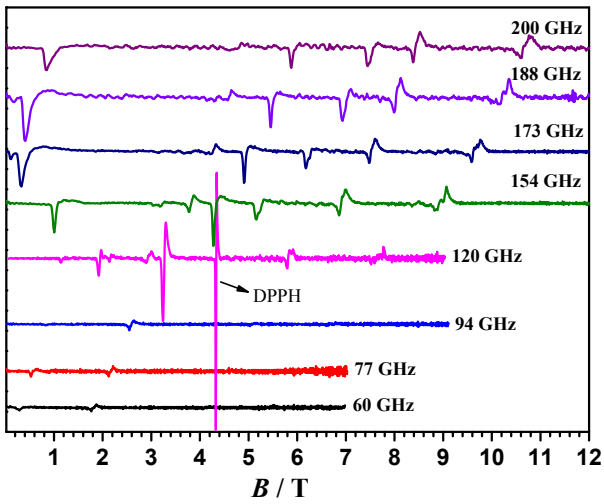


**Figure S18**. Variable-frequency EPR spectra collected on a powder sample of **2** at 4.2 K.

## 6. Theoretical Calculations

In order to obtain a further understanding, theoretical calculations based on DFT and a multi-reference *ab initio* method were performed for the complex **1 (**Fig. S19a**)**, **2** (Fig. S19b) here. The two structures were built from crystal structures and only the positions of hydrogen atoms were optimized. This type of partial optimization was performed with BP86 functional[5] and Def2-SV(P)[6] basis set. This basis set was also used for all the subsequent calculations.

For the ZFS parameters *D* and *E* of transition metal systems, although the contribution from spin-orbit coupling (SOC) is usually considered to dominate[7], recent study has indicated that spin-spin coupling (SSC) should not be negligible[8] since its contribution may approach the magnitude of 1 $cm^{-1}$. Therefore, in our calculations of *D* and *E*, both SOC and SSC were included. DFT calculations of the SH parameters utilize the coupled-perturbed SCF approach proposed by Neese[9].

In the more sophisticated multi-reference *ab initio* method, the calculations were based on state interaction in the space of 5 quintets and 35 triplets including both spin-spin coupling (SSC) and spin-orbit coupling (SOC). This state space has been successfully applied for several $d^4$ systems including both Cr(II) and Mn(III) spin centres[8,10]. The spin-free states were obtained from state average (SA)-CASSCF of 4 active electrons and five active orbitals, i.e., SA-CASSCF (4e,5o). The reliability of this active space (4e,5o) has also been verified by previous studies of similar systems[8,10]. For the contribution of SOC to *D*, two different approaches were used: First, the way based on second-order perturbation theory ($2^{nd}$ PT) as proposed by Neese and co-workers[11]. Second, the method based on effective Hamiltonian approach (EHA) as proposed by Maurice and co-workers[12].

The *ab initio* results are shown in Table S4 and DFT results are included in Table S5. All the calculations were performed with ORCA(3.0.2) program[13].

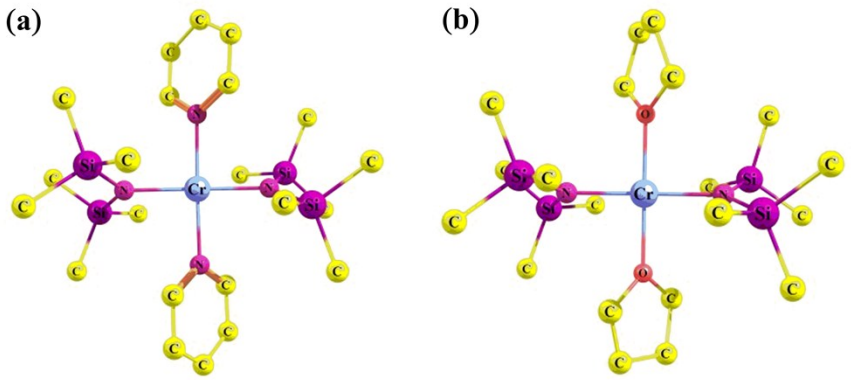


**Figure S19**. The structures used in the calculations of the SH parameters with hydrogen atoms omitted for concision. (a) Structure of complex **1** in this work. (b) Structure of complex **2** in this work.

**Table S4**. ZFS parameters obtained from *ab initio* calculations of **1** and **2** ($cm^{-1}$)

| | | SSC [a] | SOC-2nd PT [b] | SOC-EHA [c] | Sum [d] | ΔE [e] |
|---|---|---|---|---|---|---|
| Complex **1** | *D* | -0.402 | -1.485(-0.954,Q1)[f] | -1.504 | -1.888/-1.907 | 13717.7 |
| | \|*E*\| | 0.015 | 0.065 | 0.065 | 0.080/0.079 | |
| Complex **2** | *D* | -0.409 | -1.643(-1.136,Q1) | -1.664 | -2.052/-2.073 | 11644.7 |
| | \|*E*\| | 0.017 | 0.078 | 0.078 | 0.095/0.095 | |

[a] contribution of spin-spin coupling. [b] contribution of spin-orbit coupling estimated from second-order perturbation theory (2nd PT). [c] contribution of spin-orbit coupling estimated from effective Hamiltonian approach (EHA). [d] sum of SSC and SOC-2nd PT at the left side of "/", sum of SSC and SOC-EHA at the right side of "/". [e] the excitation energy of the spin-free excited eigenstate which provides the largest contribution to the SOC part of *D* within the of 2nd PT form. [f] the largest contribution to the SOC part of *D* within the of 2nd PT form is shown in the parenthesis

**Table S5**. SH parameters obtained from DFT calculations of **1** and **2** [a]

| | | BP86 | B3LYP |
|---|---|---|---|
| Complex **1** | *D* | -0.905 | -1.180 |
| | \|*E*\| | 0.022 | 0.030 |
| | $g_x$ | 1.9935 | 1.9900 |
| | $g_y$ | 1.9977 | 1.9981 |
| | $g_z$ | 1.9991 | 1.9987 |
| Complex **2** | *D* | -1.071 | -1.262 |
| | \|*E*\| | 0.031 | 0.032 |
| | $g_x$ | 1.9902 | 1.9869 |

| | | |
|---|---|---|
| $g_y$ | 1.9980 | 1.9977 |
| $g_z$ | 1.9995 | 1.9987 |

[a] both spin-spin coupling and spin-orbit coupling is included in the calculation of *D* and *E*.

Def2-SV(P) basis set is used for all the DFT calculations

**References**


(1) D. C. Bradley, M. B. Hursthouse, C. W. Newing, A. J. Welch, *J. Chem. Soc., Chem. Commun*., 1972, **9**, 567.

(2) G. M. Sheldrick. *SADABS 2.05*, University Göttingen, Germany, 2002.

(3) *SHELXTL 6.10*, Bruker Analytical Instrumentation, Madison, Wisconsin, USA, 2000

(4) (a) S. L. Wang, L. Li, Z. W. Ouyang, Z. C. Xia, N. M. Xia, T. Peng, K. B. Zhang, *Acta Phys. Sin*., 2012, **61**, 107601; (b) H. Nojiri, Z. W. Ouyang, *Terahertz Sci. Technol*., 2012, **5**, 1.

(5) (a) A. D. Becke, *Phys. Rev. A*., 1988, **38**, 3098; (b) J. P. Perdew, *Phys. Rev. B*., 1986, **33**, 8822.

(6) F. Weigend, R. Ahlrichs, *Phys. Chem. Chem. Phys*., 2005, **7**, 3297.

(7) (a) A. Abragam, B. Bleaney, *Electron Paramagnetic Resonance of Transition Ions*; Clarendon Press: Oxford, 1970; (b) J. S. Griffith, *The Theory of Transition Metal Ions*; Cambridge University Press: Cambridge, 1964; (c) V. V. Vrjamasu, E. L. Bominaar, J. Meyer, E. Münck, *Inorg. Chem.,* 2002, **41**, 6358.

(8) F. Neese, *J. Am. Chem. Soc.,* 2006, **128**, 10213.

(9) (a) F. Neese, *J. Chem. Phys.*, 2001, **115**, 11080; (b) F. Neese, *J. Chem. Phys.*, 2007, **127**, 164112.

(10) (a) Q. Scheifele, C. Riplinger, F. Neese, H. Weihe, A. L. Barra, F. Juranyi, A. Podlesnyak, P. L. W. Tregenna-Piggott, *Inorg. Chem.,* 2008, **47**, 439; (b) D. G. Liakos, D. Ganyushin, F. Neese, *Inorg. Chem.,* 2009, **48**, 10572; (c) C. Duboc, D. Ganyushin, K. Sivalingam, M. N. Collomb, F. Neese, *J. Phys. Chem. A.*, 2010, **114**, 10750.

(11) F. Neese, E. I. Solomon, *Inorg. Chem.*, 1998, **37**, 6568.

(12) R. M. Maurice, R. Bastardis, C. D. Graaf, N. Suaud, T. Mallah, N. Guihėry, *J. Chem. Theory Comput.,* 2009, **5**, 2977.

(13) (a) F. Neese, *WIREs Comput. Mol. Sci.,* 2012, **2**, 73; (b) F. Neese and F. Wennmohs, ORCA(3.0.2)-An *ab initio*, DFT and semiempirical SCF-MO package, (Max-Planck-Institute for Chemical Energy Conversion Stiftstr. 34-36, 45470Mulheim a. d. Ruhr, Germany).